The Cryosphere Discuss., doi:10.5194/tc-2017-9, 2017
Manuscript under review for journal The Cryosphere
Discussion started: 14 March 2017

The Cryosphere Discussions
Open Access
EGU

A trace gas method of evaluating interstitial air advection and diffusion in snow

Stephen A. Drake[1], John S. Selker[2], Chad W. Higgins[2]

[1]College of Earth, Ocean and Atmospheric Sciences, Oregon State University, Corvallis, 97333, USA
[2]Biological and Ecological Engineering, Oregon State University, Corvallis, 97333, USA

Correspondence to: Stephen A. Drake (stephenadrake@gmail.com)

Abstract. Atmospheric pressure gradients and pressure fluctuations drive within-snow air movement that enhances gas mobility through interstitial pore space. The magnitude of this enhancement in relation to snow microstructure properties cannot be well predicted with current methods or validated relationships. In a set of field experiments we injected a dilute mixture of 1% carbon monoxide and nitrogen gas of known volume into the topmost layer of a snowpack and, using a distributed array of thin film sensors, measured plume evolution as a function of wind forcing. We found enhanced dispersion in the streamwise direction and also along low resistance pathways in the presence of wind. These results suggest that atmospheric constituents contained in snow can be anisotropically mixed depending on the wind environment and snow structure, having implications for surface snow reaction rates and interpretation of firn and ice cores.

1 Introduction

Atmospheric pressure changes stimulate air movement in near-surface snow pore space (Clarke et al., 1987) that redistribute radiatively and chemically active trace species such as O_3 (Albert et al., 2002), OH (Domine and Shepson, 2002) and NO (Pinzer et al., 2010) thereby influencing their reaction rates. Wind blowing steadily over surface features generate localized, quasi-static pressure gradients and air in snow moves in response to these wind-induced pressure gradients (Colbeck, 1989). These topographically induced pressure gradients induce quasi-stationary circulation patterns that transport gases (Massman, 2006) and form zones of preferential sublimation and deposition (Albert, 2002). Turbulently generated pressure fluctuations also induce air movement in snow (Drake et al., 2016).

Similar to turbulence, advection through a mechanically dispersive medium such as snow dissipates a concentration gradient but in this case preferentially spreads a plume more aggressively in the downstream direction. In a wind tunnel experiment Clifton et al. (2008) found that wind directly influences air movement only within the top few millimetres of a flat, permeable medium and thereby ruled out shear as a production mechanism for in-snow advection. That is, wind does not "blow through the snow" over a flat snow surface. Quasi-static pressure gradients and transient, anisotropic pressure perturbations that induce air movement remain viable advection production candidates. The presence of in-snow advection has been experimentally inferred from temperature changes caused by forced ventilation Albert and Hardy (1995), Sokratov

The Cryosphere Discuss., doi:10.5194/tc-2017-9, 2017
Manuscript under review for journal The Cryosphere
Discussion started: 14 March 2017

and Sato (2000) and from CO_2 flux measurements (Bowling and Massman, 2011) but few measurements of natural air advection in snow have been obtained (Albert and Shultz, 2002; Huwald et al., 2012). Dispersion enhancement due to advection through interstitial pore space influences the distribution of reactive interstitial gases yet this process remains poorly understood. Step changes in permeability between successive snow layers further complicate the relationship between wind forcing and the in-snow advective response (Albert, 1996). To minimize the complicating influence of snow layering, we confined this exploration to the topmost snow layer that had been deposited by a significant snowfall event. Therefore, the purpose of this investigation is to better understand the effect that wind blowing over snow has on air movement within the topmost layer of a snowpack.

2 Methods

Our strategy is to compare model simulations that implement a solution of the advection/diffusion equation for homogenous, permeable media with experimental measurements of dispersion of a tracer gas in snow. As our measurements will show, a distinct snow layer is not homogenous and this method will highlight macroscopic channels of inhomogeneity. For the field experiments, we released a known volume of carbon monoxide (CO) at a known location in a surface snow layer and measured plume evolution with in situ sensors mounted on pickets. Consistent with Huwald et al. (2012), we chose CO as a tracer gas because its molecular weight is very close to that of air so it is nearly neutrally buoyant. Additionally, CO can be safely handled, has low background concentration and low water solubility. This latter consideration is important because snow grains may be coated with a thin film of liquid water, even at sub-freezing temperatures. Neutral buoyancy ensures that gravitational effects do not influence plume evolution, although neutral buoyancy is not strictly achieved for this experiment. A mixture of 1% CO in 99% N_2 provided sufficient concentration for sensor detection. Still, at this low concentration CO can cause unhealthy side effects in large volumes, necessitating small volume releases. Though not available in our tests, we would recommend others employing this method to blend the CO with standard air rather than N_2, which would then be essentially neutrally buoyant.

The measurement network was composed of 28 thin-film Applied Sensor MLC carbon monoxide sensors with detection range spanning four orders of magnitude (from 0.5 to 500 ppmv). To measure CO gas at well-known positions in the snow, seven CO sensors were mounted in 15-cm intervals on each of four tapered poles (or snow pickets, Fig 1). The pickets were inserted horizontally into the snow forming a rectangular sensor grid. Silicone tubing strung down the center of each picket to an outlet opposite the CO sensors provided a means to deliver the CO gas to a well-known position in the snow. This same system was also used in Huwald et al. (2012), and we refer readers to that document for a thorough explanation of materials, manufacturing and wiring requirements.

Data from the 28 CO sensors were acquired on two synchronized Campbell Scientific CR1000 loggers at 1-minute intervals. Release volume was measured with an Aalborg GFM17 Mass Flowmeter (range 0-15 SLPM) for cases 1 through 11 and with a Precision Sample Magnum Series 500 ml gas tight syringe for cases 12 through 14. CO gas was delivered fast enough

relative to the 1-minute measurement interval to approximate an instantaneous release. During each deployment four snow pickets were inserted horizontally such that we could capture horizontal variability of dispersion characteristics in snow. A Campbell Scientific Irgason ultrasonic anemometer captured 3-D wind components at 20 Hz approximately 1 m above the snow. Minutely wind speed and direction averages were computed by post-processing the high-frequency data. The experiment configuration is presented as a schematic diagram in Fig. 2.

2.1 Site description

The system represented in Fig. 2 was deployed at three locations: Santiam Pass, Oregon (elevation: 1468 m); Dutchman Flat Sno-Park, Oregon (elevation: 1905 m); and Storm Peak Lab (SPL), Mt. Werner, Colorado (elevation: 3220 m) during winter and spring seasons of 2014 and 2015. These sites span a broad range of wind forcing and snow permeability regimes. The Santiam Pass and Dutchman Flat sites were nearly flat, while the SPL deployment site was located on a slope that gradually sloped downhill to the west. Each deployment had a sonic anemometer mounted at ~ 1-m on a low-profile tower with the sonic transducer facing into the prevailing wind. The windward side of the tower was kept free of disturbance. At each site we carefully dug a low-profile snowpit, exposing a clean face into which we inserted the sensor-mounted pickets. Once the pickets were placed, we backfilled the snowpit with fresh snow and smoothed the surface to match the surrounding, undisturbed snow level. Lab-based sensitivity tests in a calibration chamber revealed that AS-MLC CO sensors are both temperature and humidity sensitive so we allowed approximately 30 min for sensor equilibration prior to a gas release. In Huwald et al. (2012) sensor pickets were placed vertically and the authors noted leakage around the picket perimeter that manifested as enhanced dispersion along the picket axis for low snow density releases. Even with horizontal (and buried) picket placements we observed indication of leakage for a few cases but most cases were performed in relatively high-density, spongy snow that seated snugly against the pickets, minimizing leakage.

2.2 Deployment description

Data were selected from a larger data set composed of 24 releases in 10 different snow conditions over two field seasons. Quality control criteria excluding some data were weather-related instrument issues such as sonic anemometer transmission losses due to snow/rain/riming, excessive gas leakage around the release picket, gas leakage at a tube fitting, and excessive icing/wetting/temperature changes of CO sensors. The dual requirements that the CO sensors needed to be ice-free with minimal temperature variations for optimal operation restricted deployment time spans to no more than several hours. Between deployments the sensors were air-dried in a lab environment to return them to an optimal operational state. Immediately prior to each deployment, we determined the prevailing wind direction so that the pickets could be inserted approximately perpendicular to the wind direction. This orientation maximized the sensor network's ability to resolve a plume propagating downwind and was achieved for all cases except cases 13 and 14, which experienced a wind shift during instrument setup. With the exception of case 12 the surface snow layer was deposited by a single storm event and was

sufficiently deep to position the sensor pickets in a homogenous snow layer. Cases 7 through 11 were acquired in a snow layer that had undergone equilibrium snow metamorphism forming spheroidal snow grains.

2.3 Calibration

We built a calibration chamber into which we could simultaneously place all 4 pickets and verify the operational capabilities of the Applied Sensor MLC CO sensors that we used for this experiment. We found through trial and error that the CO sensors are sensitive to both humidity and temperature. Furthermore, we found that sensor sensitivity decreases when exposed to the same CO concentration over a long period (> 10 minutes). To overcome these deficiencies we transported the calibration chamber to the Santiam Pass and Storm Peak Lab field sites for two snow regimes (cold snow and warm snow) and calibrated the picket-mounted CO sensors onsite. The procedure was to shovel some snow into the chamber then insert the pickets into support collars that suspended the pickets in the chamber above the snow. The chamber was sealed and a measured volume of CO introduced. A fan inside the calibration chamber facilitated thoroughly mixing the air. Measurements were acquired at 1-minute intervals with two CR1000 Campbell Scientific loggers until sensor response was documented. The chamber was then opened on both ends and allowed ~ 30 minutes for the chamber to fully evacuate. This procedure was repeated for the next measurement. This calibration procedure was time consuming and therefore we were not able to perform it in concert with field deployments. Cases 1-11 were calibrated using a warm snow calibration and cases 12-14 were calibrated with a cold snow calibration. Although the maximum recommended operating concentration is 500 ppmv, tests revealed a linear response that consistently exceeded 1000 ppmv. Measured gas concentration at the sensor nearest the release point typically exceeded 1000 ppmv but this sensor was not used for analysis and therefore did not influence experimental results. Further calibration details can be found in Huwald et al. (2012).

3 Data analysis

The results presented in this paper are based on 14 CO releases selected from five snow conditions detailed in Tables 1 and 2. With the exception of case 12, pickets were placed in a layer of snow generated by a single snow event such that we could minimize the effect of snow layering on dispersion. This requirement restricted the depth within which we placed the snow pickets. For case 12, the pickets were placed below an ice layer that was overlain by surface snow generated by a single storm event.

We used two methods to analyze the results. For the first method, we applied calibration coefficients from either warm or cold snow calibrations to voltage measurements and derived CO concentration for each sensor at each time step. From these data we calculated the position of the centroid of mass in order to determine plume propagation speed. In the second method, we calculated the time required to reach maximum concentration at each sensor as a measure of plume propagation. Deviations from the modeled concentration give a measure of the influences of advection and snow heterogeneity.

A solution of the 3-D advection/diffusion equation for a point source is (Socolofsky and Jirka, 2005):

The Cryosphere Discuss., doi:10.5194/tc-2017-9, 2017
Manuscript under review for journal The Cryosphere
Discussion started: 14 March 2017

$$C(x,y,z,t) = \frac{M}{4\pi t\sqrt{4\pi t D_x D_y D_z}} \exp\left[-\frac{((x-x_1)-Ut)^2}{4tD_x} - \frac{((y-y_1)-Vt)^2}{4tD_y} - \frac{(z-z_1)^2}{4tD_z}\right]. \quad (1)$$

If we assume horizontal snow homogeneity (constant $D_{x,y}$) then we can differentiate Eq. (1) with respect to time and set this result equal to zero to find the streamwise advection velocity:

$$\sqrt{U^2+V^2} = \sqrt{\frac{r^2-6Dt_{MAX}}{t_{MAX}^2}}. \quad (2)$$

For zero wind velocity:

$$D = \frac{r^2}{6t_{MAX}}. \quad (3)$$

Equation (3) permits calculation of the horizontal diffusion coefficient as a function of the time required between the initial release and the maximum measured concentration at each sensor location, assuming zero air velocity in snow. Non-zero interstitial air velocity and snow heterogeneity manifest as spatial variations in diffusion coefficient. We calculated the diffusion coefficient for each sensor and subtracted these values from those given by Eq. (3) to derive a residual that is an approximation of wind-driven dispersion enhancement. This technique has the advantage that absolute concentration is irrelevant so the result is insensitive to sensor calibration error.

3.1 Caveat

We will not attempt to compare the vertical diffusion coefficient with the horizontal diffusion coefficient, as that comparison would require a 3-dimensional measurement network. Riche and Schneebeli (2012) found that snow anisotropy causes differences in horizontal and vertical thermal conductivities, which suggests differences between horizontal and diffusion coefficients for CO in snow. We postulate that vertical diffusion enhancement increases as wind ventilation increases (Albert and Shultz, 2002). For this reason, we expect that our computations of horizontal diffusion will be systematically low, the degree to which depends on the difference between the horizontal and vertical diffusion coefficient and the relative wind enhancement of horizontal and vertical diffusion coefficients.

4 Results

4.1 Model simulations

Results from an advection/diffusion model assuming isotropic media with a diffusion constant of 2.56 x 10^{-5} m^2 s^{-1} consistent with snow (from Huwald et al., 2012) are shown in Fig. 3a. An instantaneous release at the origin spreads in time and the red dots mark the locations of point measurements at 15 cm, 30 cm and 45 cm from the release point. Half-hour time series of the simulated concentrations at these three locations are shown in Fig. 3b. The timeseries in Fig. 3b delineate “breakthrough curves” that have a distinctive shape with a rapidly rising concentration to a peak followed by gradual decay. In a purely

diffusive environment the breakthrough curve of each successively distant point from the release location is contained within curves defined by closer points as in Fig. 3b. Isotropic molecular diffusion spreads a plume in all directions but the centroid of mass remains stationary over time. On the other hand, advection translates the centroid. In Figs. 3c and 3d we have imposed an advective flow of 0.5 mm s^{-1} oriented along the positive x-axis. For the corresponding set of breakthrough curves in Fig. 3d, the traces cross at some point in time if advection is sufficiently fast relative to diffusion. By comparing breakthrough curves derived from field experiments with simulations we can determine the relative influences of dispersive processes. In this idealized description we do not account for snow heterogeneity, which enhances diffusion in regions of higher porosity, potentially leading to centroid displacement.

4.2 Breakthrough curves

In Fig. 4 we plotted the results of CO release R2 on March 26, 2015 (case 14 in Table 1) in the presence of moderate wind and mid-to-low density snow. The breakthrough curves are smooth and indicative of diffusion-dominated dispersion yet a subtle advection signature of breakthrough curves crossing each other is evident in Fig. 4b, similar to Fig. 3d. This result shows that an advection signature is evident at approximately 20 cm depth in mid-to-low density snow. The maximum concentration measured at the release point in Fig. 4a exceeded the linear calibration range of the CO sensors. Calibration range exceedance near the release point commonly occurred during releases but the results presented in this paper do not rely upon release point concentration measurements. Rather, larger releases enabled greater resolution of far field concentration and t_{MAX} measurements.

4.3 Effect of wind direction

For two contrasting cases during the same deployment (April 19th, 2014), Figs. 5a-d show the effect of wind on subsurface plume evolution. In case 8 (Figs. 5a-b), prevailing winds were persistent and from the west whereas for case 11 (Figs. 5c-d) winds were light and variable. The time required to reach the maximum concentration for each sensor as described in Eq. (1) is plotted in Figs. 5b and 5d. For case 8 (Fig. 5b) the plume orients streamwise to the wind with increased streamwise dispersion relative to cross-stream. The plume shape in low wind case 11 (Fig. 5d) is more circular as would be expected for diffusion-dominated dispersion. We attribute deviations from radial symmetry for low-wind case 11 to snow inhomogeneities. This case comparison shows that an advective signature is evident in at 9 cm depth in dense (430 kg m^{-3}) snow.

The subtle, streamwise plume alignment evident in Fig. 5a-b is more easily discriminated with larger CO releases, an example of which is plotted in Fig. 5e-f. This release was too large to approximate a point release but it unambiguously shows that the plume aligns in a streamwise orientation. Preferential streamwise dispersion was duplicated for subsequent large releases with persistent prevailing winds (cases 8 and 9, not shown). In-snow, streamwise plume alignment under a persistent wind regime is an unsurprising result that nevertheless bears reporting because previous studies have lacked a sufficiently dense sensor network to resolve it.

The Cryosphere Discuss., doi:10.5194/tc-2017-9, 2017
Manuscript under review for journal The Cryosphere
Discussion started: 14 March 2017

4.4 Plume propagation given by centroid of mass

We calculated the displacement of the centroid of mass at each time step as an indicator of advection. The centroid of mass is a more stable measure of plume propagation than the maximum concentration location because the latter may vacillate at each time step when two measurements are nearly the same. In Fig. 6a we plotted the position of plume centroid relative to release position for case 13, color coded by minute since release. The black asterisk marks the release point. Circles delineate centroid position at each minute and the circle diameter is a relative measure of the plume standard deviation. Triangles in Fig. 6a indicate anticipated minutely translation given by wind direction at 1/1000 of the wind speed. This multiplicative factor (1/1000) reduces wind speed to on the order of mm s^{-1}, the approximate order of magnitude for air advection in snow (Huwald et al., 2012). We do not account for the mass that advects out of the measurement network because we lack 3-dimensional measurements needed to simultaneously constrain mass loss in the vertical and horizontal directions. Instead, we assume that the centroid position in the horizontal plane is accurate over a short timespan between the initial release and the time at which mass starts to advect out of the perimeter of the measurement network.

For the initial several minutes after the release, the calculated centroid position was indeterminate because the sensor at the release position had saturated, returning NaN values. After several minutes more sensors detected the plume so the centroid position stabilized as it propagated downwind. While propagating downwind some of the plume mass concurrently propagated vertically, out of the sensor network plane. We anticipate that horizontal diffusion was slowed to the degree that the vertical diffusion coefficient exceeded the horizontal diffusion coefficient and the center of mass of the buoyant plume lifted. Numerical simulations similar to those shown in Fig. 3 but using a vertical diffusion coefficient that decreases with snow depth (not shown) are consistent with this hypothesis. After approximately 13 minutes, the calculated centroid position was driven by the CO mass still in the horizontal plane and within the sensor network and the centroid of mass appeared to stall because the smaller horizontal footprint of the upward moving plume. For the time span between 3 min and 13 min, the center of mass advected 6 cm giving an average velocity of 1.0×10^{-4} m s^{-1}, consistent with 1.2×10^{-4} m s^{-1} reported by Huwald et al. (2012) for higher permeability (lower density) snow.

To further assess the influence of wind on plume propagation we calculated the angle between the propagation of the center of mass and that given by wind direction, again assuming the wind-driven advection speed was ~1/1000 of the wind speed. Results for 4 representative cases are shown in Fig. 6b. In low-density snow and moderate wind speeds (case 13), wind direction was a good predictor for plume propagation direction, even at approximately 20 cm depth. In denser snow and moderate wind speeds (case 8) wind direction remained a good predictor for plume propagation direction with the exceptions that several minutes were required for the plume centroid position to stabilize (as noted in Fig 6a) and after ~ 13 minutes at which time snow heterogeneity and vertical dispersion conspired to degrade the correlation between wind direction and center of mass propagation direction. For case 11, in which snow density was high and winds were light and variable, the angle between wind direction and plume propagation as indicated by the center of mass was larger and highly variable. For case 12, in which low-density snow overlaid an ice layer, the plume diverged into several preferred pathways (see Section

4.5) but the centroid of mass generally advected downwind. These results show that centroid of mass propagates downwind more reliably in lower density snow than in dense snow but centroid of mass propagation direction is not necessarily a reliable indicator of the evolution of the plume footprint.

4.5 Snow layering

With the exception of case 12, we deployed our equipment in the topmost layer of a significant snowfall event to minimize the influences of snow layering on plume evolution. We include case 12 because an 18 cm new snowfall event overlaid a thick (~5-10 mm) and pervasive layer of refrozen ice, providing an unusual opportunity to study the dispersion signature below a buried, ~ impervious layer where one might expect no advection. The CO sensor-mounted snow pickets were placed at roughly 18 cm depth, just below the ice layer. Surface snow was unevenly distributed over the ice layer so picket depths varied by up to 5 cm but all pickets were positioned at the same depth below the ice layer. Winds were persistently strong from the west (blowing left to right in Fig. 7) during this release. Plume evolution for this case indicates that dispersion had not only molecular diffusion and directional wind signatures but was also strongly characterized by preferential flow regions. We hypothesize that the tracer gas was preferentially following incipient cracks and more porous pathways in the snow layer. This hypothesis is supported by Nachshon et al. (2012) who found that fractures in soil increase permeability by several orders of magnitude and serve as preferred flow pathways in the presence of a mean background flow. From this result we conclude that pressure changes above the snow incite air movement through incipient cracks and porous zones below low permeability ice layers but with less directional influence than that seen for a surface snow layer.

4.6 Plume propagation given by time to maximum concentration

Given the previously mentioned deficiencies with computing dispersion enhancement from centroid of mass velocity, we alternatively investigate dispersion enhancement by comparing measurements with the result given by Eq. (1) using a molecular diffusivity of CO in snow, (D_{CO}), of 2.56 x 10^{-5} m^2 s^{-1} (from Huwald et al., 2012). We note that diffusivity of a gas in snow varies with temperature, pressure and snow state. However, these parameters do not vary significantly for different cases obtained during a given experiment deployment. We use the measured diffusivity, $D(t_{MAX})$, and D_{CO} to estimate the Péclet number:

$$Pe = \frac{advective\ transport\ rate}{diffusive\ transport\ rate} = \frac{D(t_{MAX}) - D_{CO}}{D_{CO}}. \quad (2)$$

In Equation (2), we note that measured $D(t_{MAX})$ includes influences of both molecular diffusion and advection so one must subtract the diffusive component from the measured $D(t_{MAX})$ to derive the advective component. Since the plume is preferentially spreading vertically, mass is lost from the horizontally oriented measurement network, systematically increasing t_{MAX} values and thereby decreasing measured effective diffusivity to values smaller than molecular diffusivity. To

The Cryosphere Discuss., doi:10.5194/tc-2017-9, 2017
Manuscript under review for journal The Cryosphere
Discussion started: 14 March 2017

compensate for the systematic depression of measured effective diffusivity, we find the difference between the smallest measured effective diffusivity and the molecular diffusivity and normalize measured effective diffusivity by this difference:

$$Pe_{norm} = \frac{D(t_{MAX})+[\,D_{CO}-MIN(D(t_{MAX}))]-D_{CO}}{D_{CO}} = \frac{D(t_{MAX})-MIN(D(t_{MAX}))}{D_{CO}}. \quad (3)$$

Our rationale for applying this normalization is that the diffusivity of a gas in snow can be no less than the molecular diffusivity. This normalized Péclet number no longer represents the absolute ratio of advective to diffusive transport. But it does preserve a relative measure of advection vs. diffusion and guarantees that the normalized Péclet number is no less than zero. For example, comparing moderate-wind case 8 in Fig. 8a (see also Figs. 5a-b) with low wind case 11 in Fig 8b (see also Figs. 5c-d) we note advective signatures streamwise and also along one of the sensor pickets, indicating that leakage along a picket that is exacerbated by a wind-induced pressure gradient. The bullseye at the sensor just below the release point in Fig. 8b is due the large release volume rather than advection. The Pe_{norm} gradient is weak in Fig. 8b relative to Fig. 8a as one would expect for a diffusion-dominated regime. Discrepancies from radial symmetry evident in Fig. 8b indicate preferential dispersion pathways along inhomogeneities in the snow layer. Ignoring differences in sensor depth, snow microphysics, and high volume release cases (cases 4, 5, 6 and 10) the R^2 correlation was 0.61 between average wind speed and the maximum Pe_{norm} for the remaining cases. This result suggests that in-snow advection increases with wind speed and that snow state and depth in snow tempers the magnitude of in-snow advection. A three-dimensional measurement design would improve the quality of the Péclet number values and, accompanied by high-resolution snow characterization, enable absolute comparison of the advective vs. diffusive transport in both vertical and horizontal planes.

5 Conclusions

Atmospheric pressure gradients can induce subsurface advection that enhances plume dispersion, even in dense snow. Over smooth, flat reaches with a prevailing wind, a subsurface plume aligns in a streamwise orientation. Snow inhomogeneities can enhance anisotropic dispersion as wind speed increases, invalidating the notion of a mono-valued diffusion coefficient over small (1 m^2) areas. The size of a surface snow sample needed to diagnose its dispersive properties therefore varies with wind forcing and snow state. Mobile trace species near the snow surface are subject to several competing physical dispersion processes including diffusion, topographically induced circulations and advection. Each of these processes distributes mobile gas species in different ways so the fate of these trace species depends on the relative contribution of each of these processes. High resolution 3-dimensional measurements using an apparatus that minimally influences snow state are needed to account for vertical plume propagation and thereby discriminate the relative contributions of the processes that enhance dispersion in snow.

Broader implications of these findings are that dispersion in snow depends not only upon grain-scale properties but also macroscopic snow inhomogeneities. A measurement footprint must be large enough to capture the effect of patches of higher permeability snow because variability of gas dispersion in snow correspondingly increases the variation of the distribution of

interstitial gases and their reaction rates. A long timescale implication of these results is that uncertainty in trace gas distribution for replicate firn/ice cores is broadened to the degree that horizontal heterogeneity is preserved or augmented as snow accumulates and compacts.

Acknowledgements

We thank Dr. Noah Molotch and Dr. Michael Durand for organizing deployments at Storm Peak Lab, Colorado. We thank Lisa Dilley and USFS for arranging deployments in Deschutes National Forest, Oregon. Dr. Ziru Liu and Rebecca Hochreutener assisted with the field deployments. Data from these experiments may be obtained by corresponding with the first author.

Author contribution

S. Drake, J. Selker and C. Higgins designed the experiments and S. Drake performed them, assisted by Z. Liu and R. Hochreutener. S. Drake wrote the manuscript. J. Selker and C. Higgins edited it.

References

Albert, M. R.: Modeling heat, mass, and species transport in polar firn, Ann. Glaciol., 23, 138-143, doi:10.1017/S0260305500013355, 1996.

Albert, M. R.: Effects of snow and firn ventilation on sublimation rates, Ann. Glaciol., 35, 52-56, doi:10.3189/172756402781817194, 2002.

Albert, M. R., and Hardy, J. P.: Ventilation experiments in a seasonal snow cover, in: Biogeochemistry of Seasonally Snow-Covered Catchments, edited by: K. A. Tonnessen, M. A. Williams, and M. Tranter, Int. Assoc. of Hydrol. Sci. Press, Inst. of Hydrol., Wallingford, UK, 228, 41–49, 1995.

Albert, M. R., and Perron, F. E.: Ice layer and surface crust permeability in a seasonal snow pack, Hydrol. Process., 14, 3207-3214, doi: 10.1002/1099-1085(20001230)14:183.3.CO;2-3, 2000.

Albert, M. R., and Shultz, E. F.: Snow and firn properties and air-snow transport processes at Summit, Greenland, Atmos.Environ., 36, 2789-2797, doi:10.1016/S1352-2310(02)00119-X, 2002.

Bowling, D. R., and Massman, W. J.: Persistent wind-induced enhancement of diffusive CO_2 transport in a mountain forest snowpack, J. Geophys. Res., 116, G04006, doi:10.1029/2011JG001722, 2011.

Clifton, A., Manes, C., Ruedi, J. D., Guala, M., and Lehning, M.: On shear-driven ventilation of snow, Bound.-Lay. Meteorol., 126, 249–261, doi:10.1007/s10546-007-9235-0, 2008.

Domine, F. and Shepson, P. B.: Air-snow interactions and atmospheric chemistry, Science, 297, 1506–1510, doi:10.1126/science.1074610, 2002.

Doyle, G., and Rice, C. W.: Influence of high-frequency ambient pressure pumping on carbon dioxide efflux from soil, Agric. Forest Meteor., 124, 193-206, doi:10.1016/j.agrformet.2004.01.014, 2004.

Drake, S. A., Huwald, H., Parlange, M. B., Selker, J. S., Nolin, A. W., and Higgins, C. W.: Attenuation of wind-induced pressure perturbations in alpine snow, J. Glaciol., 62, 674-683, doi:10.1017/jog.2016.53, 2016.

Huwald, H., Selker, J. S., Tyler, S. W., Calaf, M., and Giesen, N. C. v. d.: Carbon monoxide as a tracer of gas transport in snow and other natural porous media, Geophys. Res. Lett., 39, doi:10.1029/2011GL050247, 2012.

Maier, M., Schack-Kirchner, H., Aubinet, M., Goffin, S., Longdoz, B. and Parent, F.: Turbulence effect on gas transport in three contrasting forest soils, Soil Sci. Soc. Am. J., 76, 1518-1528, doi:10.2136/sssaj2011.0376, 2012.

Merbold, L., Steinlin, C., and Hagedorn, F.: Winter greenhouse gas fluxes (CO_2, CH_4 and N_2O) from a subalpine grassland, Biogeosciences, 10, 3185-3203, doi:10.5194/bg-10-3185-2013, 2013.

Paw U, K. T., Ideris, J., Matista, A., Rolston, D. E., Hsiao, T. C., Kochendorfer, J., Wharton, S., and Pyles, R. D.: Pressure Pumping Effects on Soil Efflux Measurements of CO_2, in: Kearney Foundation of Soil Science: Soil Carbon and California's Terrestrial Ecosystems Final Report, 2006.

Pinzer, B. R., Kerbrat, M., Huthwelker, T., Gäggeler, H. W., Schneebeli, M., and Ammann, M.: Diffusion of NOx and HONO in snow: A laboratory study, J. Geophys. Res.: Atmospheres, 115, doi:10.1029/2009JD012459, 2010.

Redeker, K. R., Baird, A. J., and The, Y. A.: Quantifying wind and pressure effects on trace gas fluxes across the soil–atmosphere interface, Biogeosciences, 12, 7423-7434, doi:10.5194/bg-12-7423-2015, 2015.

Rinaldi, A. P., Vandemeulebrouck, J., Todesco, M, and Viveiros, F.: Effects of atmospheric conditions on surface diffuse degassing, J. Geophys. Res-Solid, 117, doi:10.1029/2012JB009490, 2012.

Waddington, E. D., Cunningham, J., and Harder, S. L.: The Effects Of Snow Ventilation on Chemical Concentrations, in: Chemical Exchange Between the Atmosphere and Polar Snow, edited by: Wolff, E. W. and Bales, R. C., NATO ASI Series, 43, Springer, Berlin, Germany, 403-452, 1996.

The Cryosphere Discuss., doi:10.5194/tc-2017-9, 2017
Manuscript under review for journal The Cryosphere
Discussion started: 14 March 2017

Table 1. Summary of cases used for this analysis. Wind speed is at 1-m nominal height. Layer density is the average snow density for the layer between the snow surface and measurement depth.

Case Id	Date	Release Id	Release Volume L	Layer Density kg m^{-3}	Mean wind speed m s^{-1}	Picket Spacing cm	CO Sensor depth cm
1	03 Apr 2014	R1	2.00	249	1.84	29, 36, 28	13, 14, 14, 14
2		R2	1.33		1.72		
3		R3	2.67		1.86		
4	04 Apr 2014	R3	9.50	249	2.33	11.5, 13.5, 16	6.8, 7.0, 6.0, 6.8
5		R4	6.00		2.45		
6		R5	9.50		2.57		
7	19 Apr 2014	R1	2.30	430	2.63	15.0, 17.6, 17.0	9.0, 9.6, 9.0, 9.0
8		R2	4.00		2.02		
9		R3	5.00		1.55		
10		R4	6.67		0.70		
11		R5	1.17		0.34		
12	24 Mar 2015	R1	0.20	Variable, ice layer	3.91	15.5, 14.5, 15.0	21.0, 19.0, 16.0, 17.0
13	26 Mar 2015	R1	0.20	227	3.26	19.0, 19.0, 18.0	18.0, 19.0, 19.0, 19.0
14		R2	0.20		2.92		

The Cryosphere Discuss., doi:10.5194/tc-2017-9, 2017
Manuscript under review for journal The Cryosphere
Discussion started: 14 March 2017

Table 2. Deployment summary of meteorological and snow conditions.

Date	Location	Meteorological and Surface Snow Conditions. Air Temperature; Crystal type; Size; Hardness
03 Apr 2014	Dutchman Flat, Oregon	Strong winds, predominantly from the SW with arrival of a surface front. Intermittent snowfall through the night. T_{AIR} ranged -1 to 1 C; faceted crystals; coarse; 2F
04 Apr 2014	Dutchman Flat, Oregon	Winds turning from SW to NW through the day. Less turbulent and low directional variability. Clearing weather through day. T_{AIR} ranged -1 to 0 C; faceted crystals; coarse; 2F
19 Apr 2014	Santiam Pass, Oregon	Clear day. T_{AIR} ranged -2 to 5 C; rounded grains, very coarse; 4F
24 Mar 2015	Storm Peak Lab, Colorado	Stormy with strong winds. T_{AIR} ranged -7 to -5 C; faceted crystals; medium; 3F
26 Mar 2015	Storm Peak Lab, Colorado	Clear day. T_{AIR} ranged -5 to -2 C; faceted crystals; medium; 2F

The Cryosphere Discuss., doi:10.5194/tc-2017-9, 2017
Manuscript under review for journal The Cryosphere
Discussion started: 14 March 2017

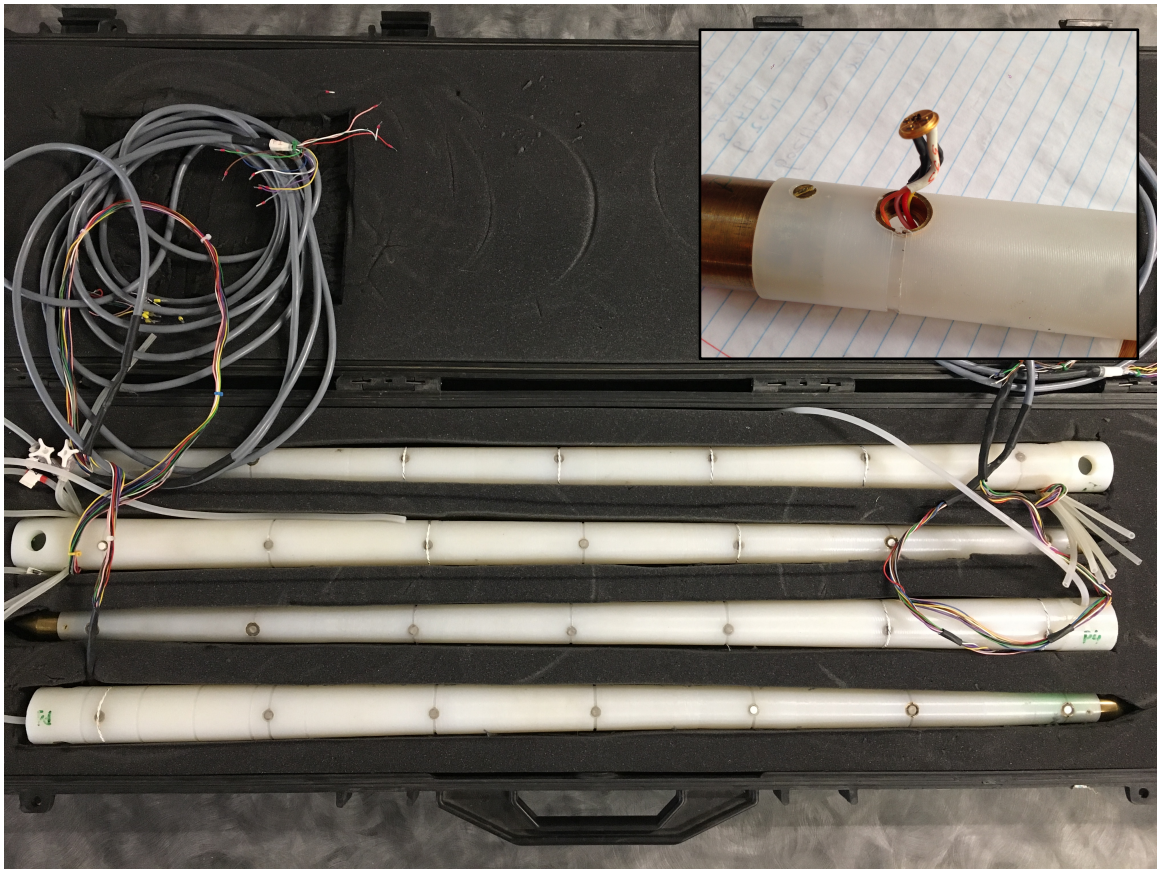

Figure 1. Four 1 m snow pickets, each mounted with 7 CO sensors at 15 cm spacing. In the inset, a close-up picture of a single sensor before flush mounting.

The Cryosphere Discuss., doi:10.5194/tc-2017-9, 2017
Manuscript under review for journal The Cryosphere
Discussion started: 14 March 2017

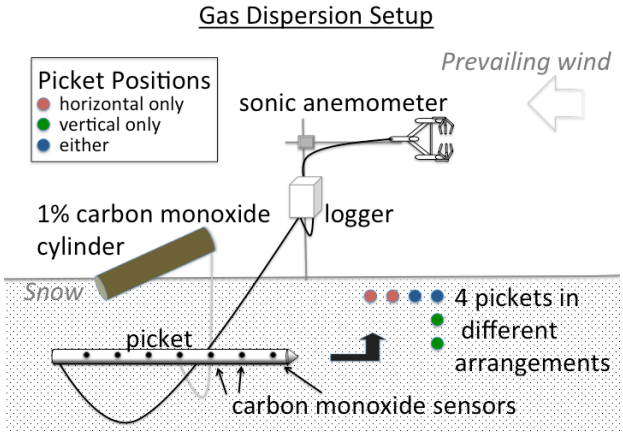

Figure 2. Diagram of the experimental setup showing relative positions of the sonic anemometer and snow pickets. This experiment documents results using the horizontal picket configuration.

The Cryosphere Discuss., doi:10.5194/tc-2017-9, 2017
Manuscript under review for journal The Cryosphere
Discussion started: 14 March 2017

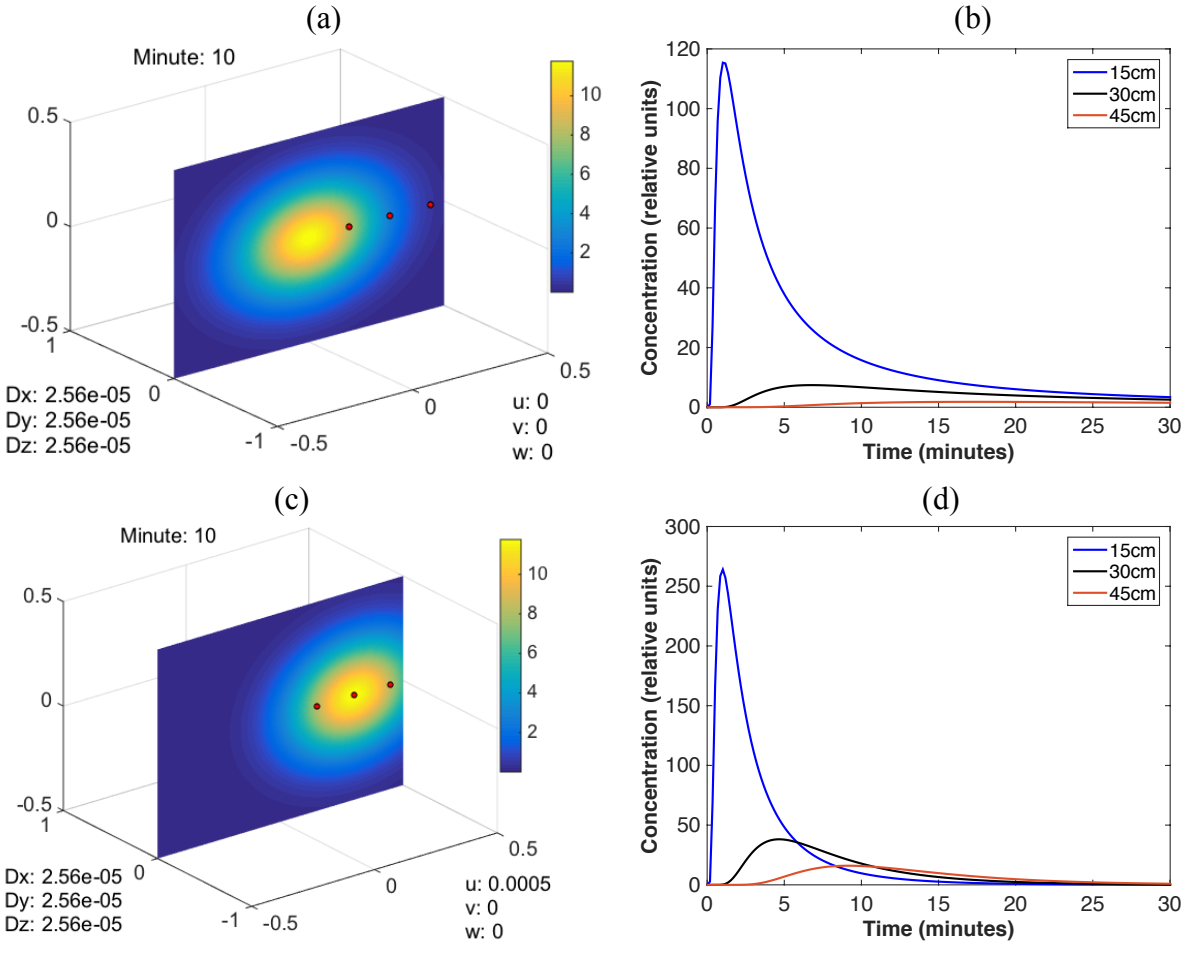

Figure 3. Vertical cross-section of simulated plume dispersion in a purely diffusive case over a 1 m^3 volume (panel *a*, upper left) and the associated breakthrough curve (panel *b*, upper right) and for a diffusive/advective case (panel *c*, lower left) with associated breakthrough curve (panel *d*, lower right). For the advective/diffusive scenario, plume concentration is greater at the 30-cm position than the 15-cm position after 10 minutes.

The Cryosphere Discuss., doi:10.5194/tc-2017-9, 2017
Manuscript under review for journal The Cryosphere
Discussion started: 14 March 2017

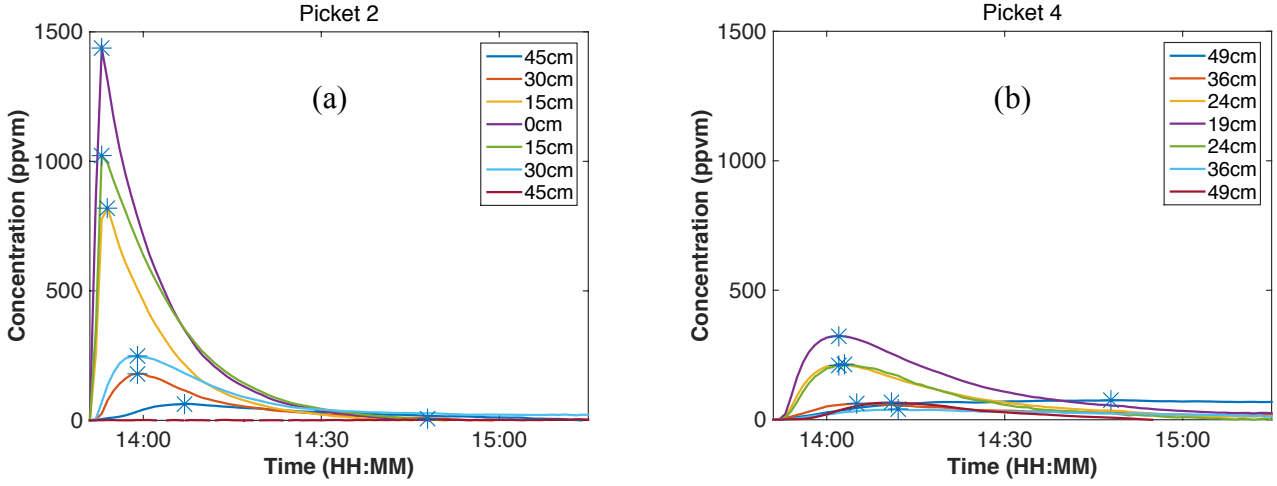

Figure 4. Calibrated near-field break-through curves for case 14 (panel *a*) and 19 cm downstream of the release point (panel *b*). CO concentration data were acquired at 1-minute resolution. The CO gas release position is on picket 2, shown in panel (*a*), on the opposite side of the picket from the mid-picket (0 cm) sensor. Distances given in the legend are measured from the release point to the given sensor for both figures. Blue asterisks highlight time of maximum concentration at that position.

The Cryosphere Discuss., doi:10.5194/tc-2017-9, 2017
Manuscript under review for journal The Cryosphere
Discussion started: 14 March 2017

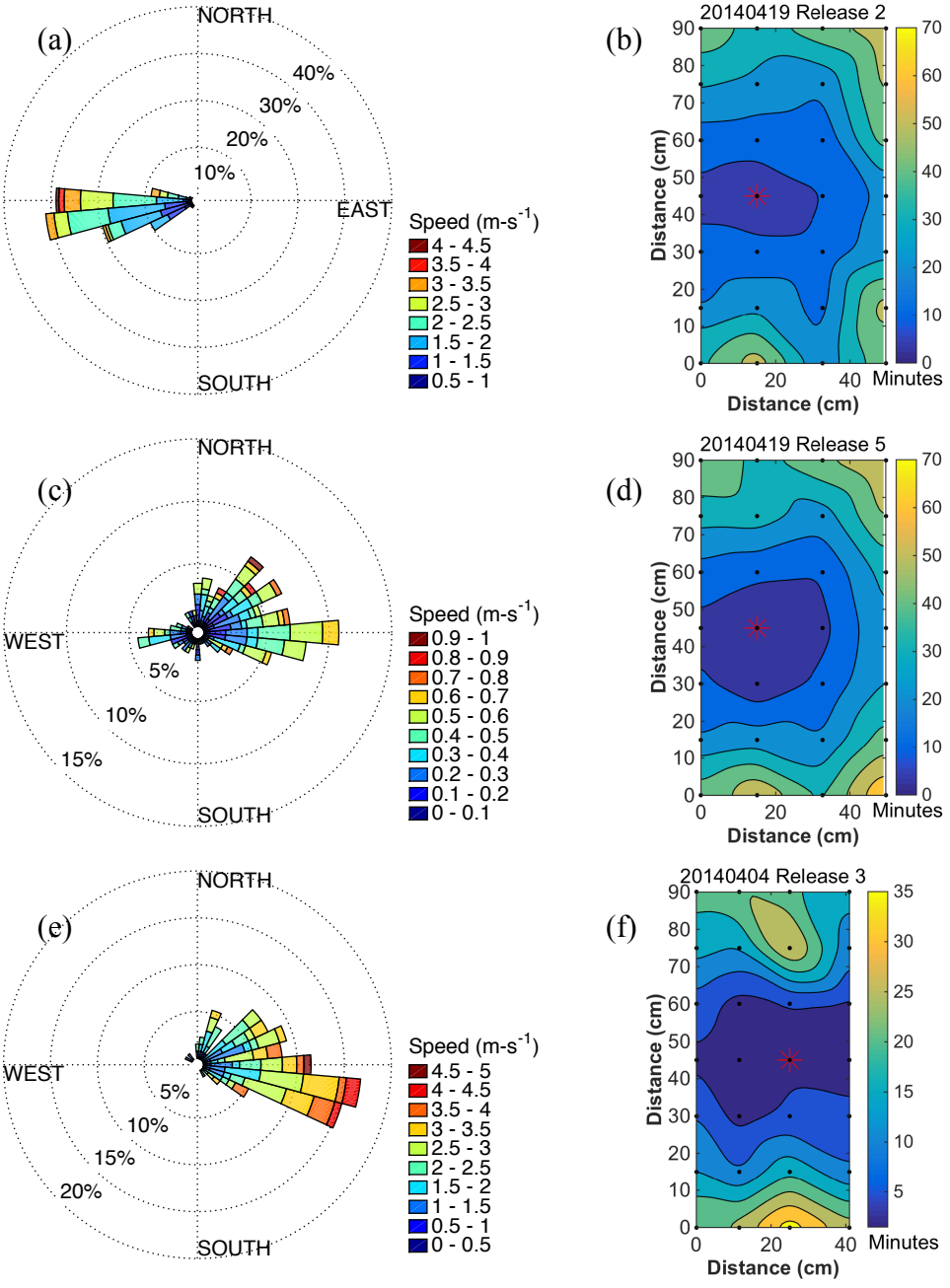

Figure 5. Windrose for persistent wind case 8 in high-density snow (a), for light, variable wind case 11 also in high-density snow (c) and for persistent wind with medium density snow case 4 (e). Winds are plotted relative to picket axis. Wind speed is color coded with speed ranges given in the legend. Time to maximum concentration is color filled by minutes from release time for case 8 (b) and case 11 (d) and case 4 (f). Contours are in 10-minute increments for (b) and (d) and 5-minute increments for (f). Sensor positions are marked as black dots and release point with red asterisks. The tops of plots (b), (d) and (f) align with the north direction of the windroses.

The Cryosphere Discuss., doi:10.5194/tc-2017-9, 2017
Manuscript under review for journal The Cryosphere
Discussion started: 14 March 2017

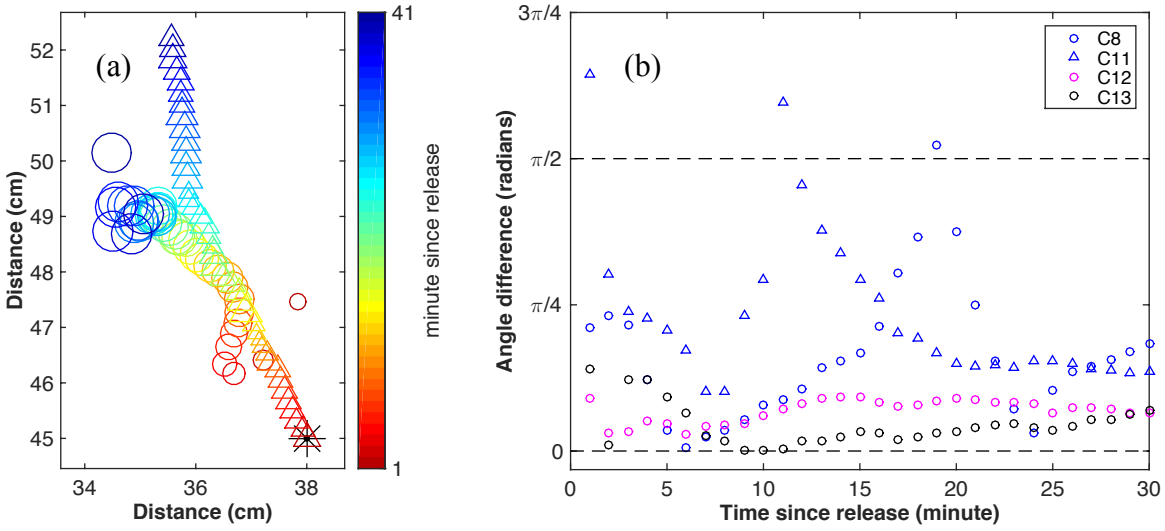

Figure 6. Centroid of mass plotted for case 13 color coded by minute since release (a). A black asterisk marks release position. In (b) the angle between the centroid of mass translation direction and the wind direction has higher correspondence in lower density snow (e.g., C13).

The Cryosphere Discuss., doi:10.5194/tc-2017-9, 2017
Manuscript under review for journal The Cryosphere
Discussion started: 14 March 2017

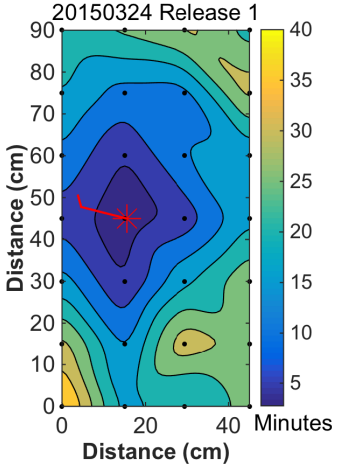

Figure 7. Plot of the time required for CO to reach maximum concentration for a release with sensor pickets placed below an ice layer. The plume has a molecular diffusion signature (roundish), a wind direction signature (downwind propagation) but also is characterized by flow along preferred pathways, which renders as irregular lobes at the sensor network resolution.

The Cryosphere Discuss., doi:10.5194/tc-2017-9, 2017
Manuscript under review for journal The Cryosphere
Discussion started: 14 March 2017

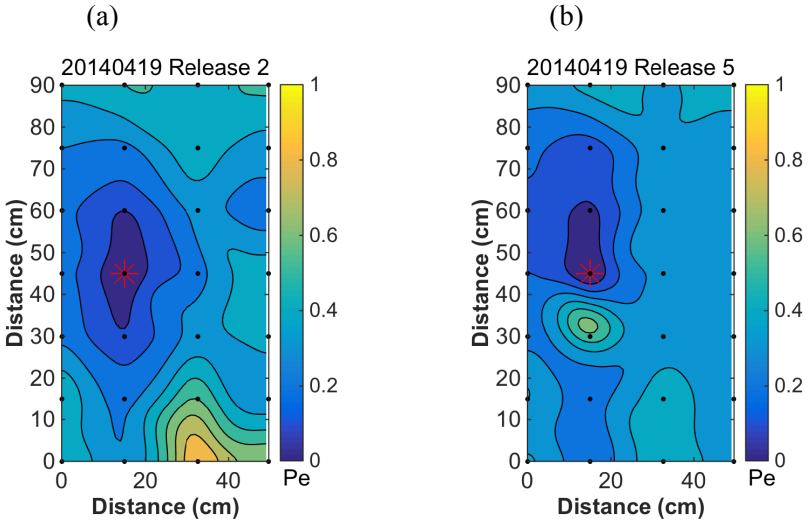

Figure 8. Normalized Péclet number for windy case 8 (panel a) and low-wind case 11 (panel b). Both cases were obtained during the same picket deployment. Case 8 shows preferential streamwise dispersion (see also windroses in Fig. 5) as well as enhanced dispersion along low-impedance pathways. In (b), but for the anomalously large Péclet number gradient just below the release point (due to large release volume), the gradient is weak relative to (a), characteristic of a diffusion-dominated regime.